


 Cite this: *RSC Adv.*, 2025, **15**, 40381

Solid-state chemical reaction-driven BiOIO_3 catalyst for boosting piezocatalytic activation of peroxyomonosulfate toward pollutant degradation

 Yuling Ye^{abc}, Xiaorong Zeng,^a Aize Hao,  ^{abc} Zheng Fang,^{abc} Youguang Ran,^a Jiayi Zhu,^a Shanshan Hu^a and Xiaonan Liu^{abc}

A simple and scalable solid-state chemical reaction method was employed to fabricate the BiOIO_3 piezocatalyst. Notably, the BiOIO_3 piezocatalyst, in conjunction with ultrasonic vibration (US) and the peroxyomonosulfate (PMS) system, exhibited exceptional catalytic performance in the degradation of pollutants (rhodamine B (RhB) and tetracycline (TC)). The BiOIO_3 /PMS/US system achieved an impressive reaction rate constant (RhB dye: 0.4958 min^{-1} and TC: 0.1983 min^{-1}) and high degradation efficiency (RhB dye: 88.8% within 4 min and TC: 86.3% within 10 min) and demonstrated good stability, surpassing the performance of the single BiOIO_3 and other material systems. Radical quenching and EPR spectroscopy experiments further identified the contributions of non-free radicals and free radicals in the BiOIO_3 /PMS/US system. Finally, a mechanism was proposed for the BiOIO_3 /PMS/US system. This work not only offers insights into the design of high-performance piezocatalysts but also advances high-efficiency approaches for sustainable wastewater remediation.

Received 19th August 2025

Accepted 8th October 2025

DOI: 10.1039/d5ra06135k

rsc.li/rsc-advances

1. Introduction

There is an increasing recognition of the significant impact of urbanization on natural aquatic ecosystems. Recently, the extensive use of chemical products in different sectors, including agriculture, medicine and urban areas, has led to the presence of organic contaminants in water bodies, posing threats to surface and groundwater resources.^{1–5} As such, there is a pressing need to explore highly efficient and cost-effective methods for wastewater treatment. The advanced oxidation processes (AOPs) have emerged as a well-established approach for the removal of pollutants from water. This process is characterized by the generation of highly reactive radicals to oxidize organic molecules into small compounds, ultimately resulting in the formation of carbon dioxide and water.^{6,7}

Piezocatalysis, as an emerging catalytic method, utilizes the property of piezoelectric materials for converting mechanical energy into chemical energy. This is increasingly recognized as an innovative approach to effectively address issues related to environmental pollutants and energy shortages.^{8–14} However, despite some advancements, piezocatalytic activity still does not

meet the application requirement. Therefore, there is an urgent need to explore an efficient strategy to develop high-performance piezocatalysts. Additionally, piezocatalysis has shown significant promise for the activation of PMS, demonstrating considerable potential for environmental purification and the reutilization of wastewater resources. Particularly, it could effectively degrade refractory organic pollutants in aqueous environments into small and less toxic molecules.^{15–17}

As a result, piezocatalysis is positioned to play a crucial role as a pre-treatment unit on AOPs and as a vital component in the future of water pollution control engineering. Its distinctive capacity to harness weak mechanical forces present in nature distinguishes it from traditional resource and energy-intensive methodologies, marking it as a transformative innovation in AOP technology. To enhance the activation of PMS, it is essential to explore more efficient materials. Additionally, developing other materials that exhibit inherent asymmetry for the piezoelectric activation of PMS has considerable potential. Modulation of the production of active species for piezocatalysis coupled with PMS is also critical. The active species involved in AOPs include a variety of free radicals (e.g. $\cdot\text{O}_2^-$ and $\cdot\text{OH}$) and non-free radicals (e.g. ${}^1\text{O}_2$). The generated radical species are electrophilic and nucleophilic, displaying relatively stable reactivity without distinct selectivity. In contrast, the produced non-radical species show electrophilic characteristics, allowing controlled reactivity strength and specific reaction selectivity. Recently, some investigations have highlighted the potential of novel material design strategies and other approaches to exert control for the production of active species.^{18–21} These

^aSchool of Chemical Engineering, Sichuan University of Science and Engineering, Zigong 643000, China. E-mail: h1061717965@163.com; lxn@suse.edu.cn

^bNational Engineering Laboratory of Circular Economy, Sichuan University of Science and Engineering, Zigong 643000, China

^cSichuan Engineering Technology Research Center for High Salt Wastewater Treatment and Resource Utilization, Sichuan University of Science and Engineering, Zigong 643000, China



advancements are promising for directing reaction pathways to achieve desired products, thus enhancing the efficiency and selectivity of piezocatalytic coupled PMS activation in addressing the complexity of organic pollutants in real water bodies.

Bismuth-based catalysts, such as BiO_x (where $X = \text{Cl}, \text{Br}$, and I), Bi_2WO_6 and BiOIO_3 , have garnered significant attention in the fields of energy conversion and wastewater purification owing to their characteristic layered structure, which endows them with exceptional physicochemical properties.^{22–27} BiOIO_3 exhibits significant advantages, such as a noncentrosymmetrical crystal structure, which facilitates charge carrier separation more effectively than other bismuth-based materials. This enhanced performance is attributed to internal electric fields generated by its layered configuration.²⁸ Moreover, the synthesis methods of bismuth-based materials are focused on solvothermal, precipitation and wet chemical reactions. Notably, the low-heat solid-state chemical reaction has emerged as an effective and facile method for preparing functional nanomaterials, as it avoids the need for solvents and complicated procedures, which is suitable for large-scale industrial production.^{29–31} Therefore, it is of interest to explore a solid-state chemical reaction method for the synthesis of BiOIO_3 and to investigate its potential applications in wastewater purification.

In this work, we employ a straightforward strategy to prepare the BiOIO_3 catalyst for the activation of PMS under external ultrasound irradiation. The system exhibits remarkable efficiency in treating wastewater pollutants. Radial quenching experiments and EPR technology confirm the presence of reactive species involved in both radical and non-radical reaction pathways during the piezocatalytic coupled PMS activation process. These results indicate that the coupled system significantly enhances PMS utilization efficiency, demonstrating superior oxidation effectiveness compared to the individual systems.

2. Experimental section

The synthesis of the BiOIO_3 catalyst was accomplished through solid-state chemical reaction and post-annealing methods. Specifically, 10 mmol of $\text{Bi}(\text{NO}_3)_3 \cdot 5\text{H}_2\text{O}$ and 20 mmol of KIO_3 were weighed and ground into a fine powder. Two reagents were then thoroughly mixed and ground for approximately 60 min. Subsequently, 4 ml of PEG400 was added to the reaction mixture. The above mixture was sealed in a conical bottle and placed in a water bath at 80 °C for 20 h to ensure complete reaction. Following this, the resultant powder was washed sequentially with distilled water and absolute ethanol. This precipitate was collected and dried. Ultimately, the desired product, BiOIO_3 , was obtained through calcining the precursor at 350 °C for 2 h. The material characterizations, piezocatalytic performance and activation of PMS for the degradation of pollutants are given in the SI in detail.

3. Results and discussion

XRD was adopted to analyze the crystal structure of the BiOIO_3 sample. Fig. 1(a) indicates that all diffraction peaks are indexed

and correspond to the orthorhombic BiOIO_3 phase (ICSD #262019).³² The presence of intense and sharp peaks demonstrates the well-crystallized nature of BiOIO_3 . Furthermore, the absence of other peaks suggests high purity.

Additionally, the chemical composition and valence states of BiOIO_3 were examined using XPS, as illustrated in Fig. S1 and 1(b–d). The XPS survey spectra confirm the presence of elements Bi, I and O in BiOIO_3 in Fig. S1. In Fig. 1(b), the high-resolution Bi 4f spectrum of BiOIO_3 shows peaks at 159.08 and 164.36 eV, which are attributed to $\text{Bi 4f}_{7/2}$ and $\text{Bi 4f}_{5/2}$ with the Bi^{3+} oxidation state, respectively.^{32,33} The I 3d XPS spectrum of BiOIO_3 presented in Fig. 1(c) displays binding energies of 623.81 ($\text{I 3d}_{5/2}$) and 635.25 eV ($\text{I 3d}_{3/2}$), corresponding to the I^{5+} oxidation state in BiOIO_3 . Finally, two peaks in the O 1s spectrum of BiOIO_3 (Fig. 1(d)) are observed at binding energies of 530.04 eV and 532.12 eV. The primary peak at 530.04 eV is attributed to lattice oxygen (O_L), associated with a stronger Bi–O bond, while the peak at 532.12 eV is attributed to surface-absorbed oxygen (O_A , $-\text{OH}$ and chemisorbed oxygen-containing species).³³ To investigate the morphology of BiOIO_3 , SEM was performed. SEM images presented in Fig. 1(e and f) reveal that BiOIO_3 exhibits an irregular plate-like two-dimensional structure, with sizes ranging from tens to hundreds of nanometers. The thickness of the BiOIO_3 nanoplates is approximately 20–30 nm.

The piezocatalytic performance of BiOIO_3 was evaluated by degrading pollutants, specifically MB and RhB dyes, under strain by ultrasonic vibration. UV-visible absorption spectra of MB and RhB dye solutions at various time intervals when using BiOIO_3 are presented in Fig. 2(a and b). The plots clearly indicate that the absorption peaks of both MB and RhB decrease over time. Notably, Fig. 2(b) demonstrates that the characteristic peak of RhB declines more rapidly than that of MB, suggesting higher degradation efficiency for RhB. The degradation curves of the various dye solutions (C/C_0 vs. time) using BiOIO_3 are illustrated in Fig. 2(c and d). It is evident that BiOIO_3 exhibits superior piezocatalytic activity in degrading RhB compared to MB.

To analyze the kinetics of the piezocatalytic degradation reaction, first-order kinetic fitting was conducted to obtain the kinetic coefficients (k). Fig. 2(e) presents kinetic coefficients (k) for the degradation of MB by BiOIO_3 under different conditions. Through fitting the data to a first-order kinetic model represented by the equation $\ln(C/C_0) = -kt$, the values of k for BiOIO_3 in the presence of MB and RhB dye solutions are calculated to be 0.00776 and 0.01215 min^{-1} . Notably, the k value for BiOIO_3 in relation to RhB is significantly higher than that for MB. Furthermore, Fig. 2(f) illustrates the degradation efficiency of BiOIO_3 for various dyes under ultrasonic vibration. The degradation efficiency for MB is 56.6%, while that for RhB is 77.3% after 120 min.

The development of efficient and straightforward approaches to activate PMS for the degradation of organic pollutants is crucial for advanced sewage treatment technology.³⁴ Thus, the application of ultrasonic vibration to investigate the piezocatalytic activation of PMS by BiOIO_3 for the degradation of pollutants is of particular interest. Fig. 3(a)



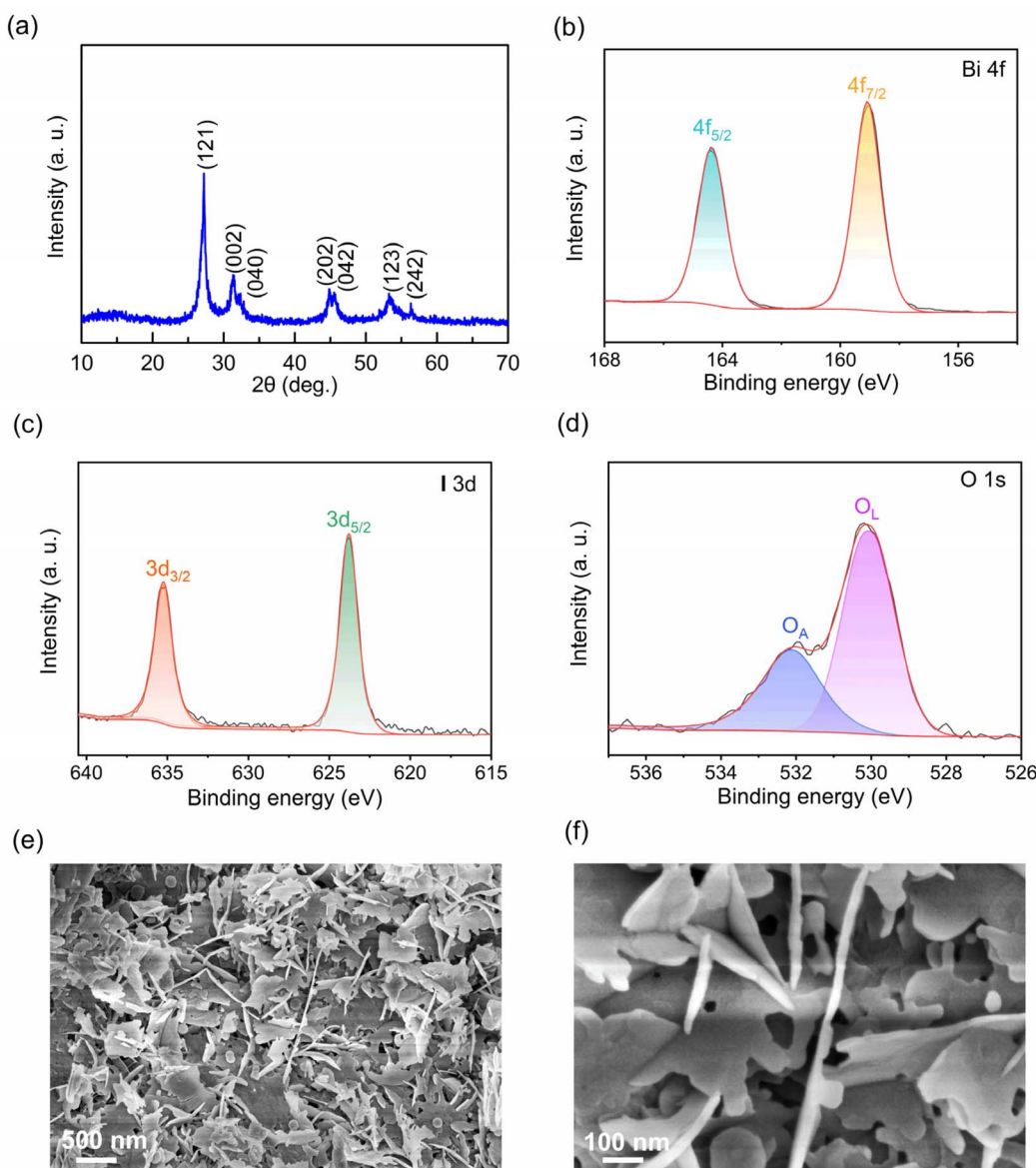


Fig. 1 (a) XRD pattern of BiOIO_3 . High-resolution XPS spectra of (b) Bi 4f , (c) I 3d , and (d) O 1s for BiOIO_3 . (e–f) SEM images of BiOIO_3 .

presents the RhB degradation curves (C/C_0 versus time) for PMS, BiOIO_3 , and the $\text{BiOIO}_3/\text{PMS}$ system under US conditions. Notably, the $\text{BiOIO}_3/\text{PMS}$ system exhibits a significantly faster degradation rate compared to either PMS or BiOIO_3 alone after just 4 min. Based on pseudo-first-order kinetic fitting, the reaction rate constant values for PMS, BiOIO_3 , and the $\text{BiOIO}_3/\text{PMS}$ system are determined to be 0.01868, 0.01247, and 0.49582 min^{-1} , as shown in Fig. 3(b). The k value for the $\text{BiOIO}_3/\text{PMS}$ system is approximately 40 times greater than that of BiOIO_3 under ultrasonic conditions.

Fig. 3(c) illustrates that the $\text{BiOIO}_3/\text{PMS}$ system achieves a degradation ratio of approximately 88.8% within 4 min, which is significantly higher than the 6.9% observed for BiOIO_3 alone. This finding indicates that ultrasonic vibration effectively induces piezocatalytic activation of PMS, facilitating the degradation of the pollutant. Compared to the individual

components, BiOIO_3/US and PMS/US treatments, the catalytic kinetics and degradation efficiency of the $\text{BiOIO}_3/\text{PMS/US}$ system are notably enhanced. This demonstrates a strong synergistic effect among BiOIO_3 , PMS, and US in the degradation of RhB, highlighting the efficacy of piezocatalytic PMS activation techniques for pollutant degradation. As reported in previous results, the synergistic effect between the catalyst and PMS improves both the pollutant degradation activity and PMS utilization efficiency.^{15,20} Consequently, piezocatalysis represents a promising and efficient method for persulfate activation in novel wastewater treatment technology. To evaluate the stability of the $\text{BiOIO}_3/\text{PMS/US}$ system, cycling tests were conducted, as shown in Fig. 3(d). The degradation ratio of the $\text{BiOIO}_3/\text{PMS/US}$ system reaches 88.8% after 4 min. Although a slight decrease in degradation ratio is observed within three cycles, this system still presents a high efficiency of 84.2%. This



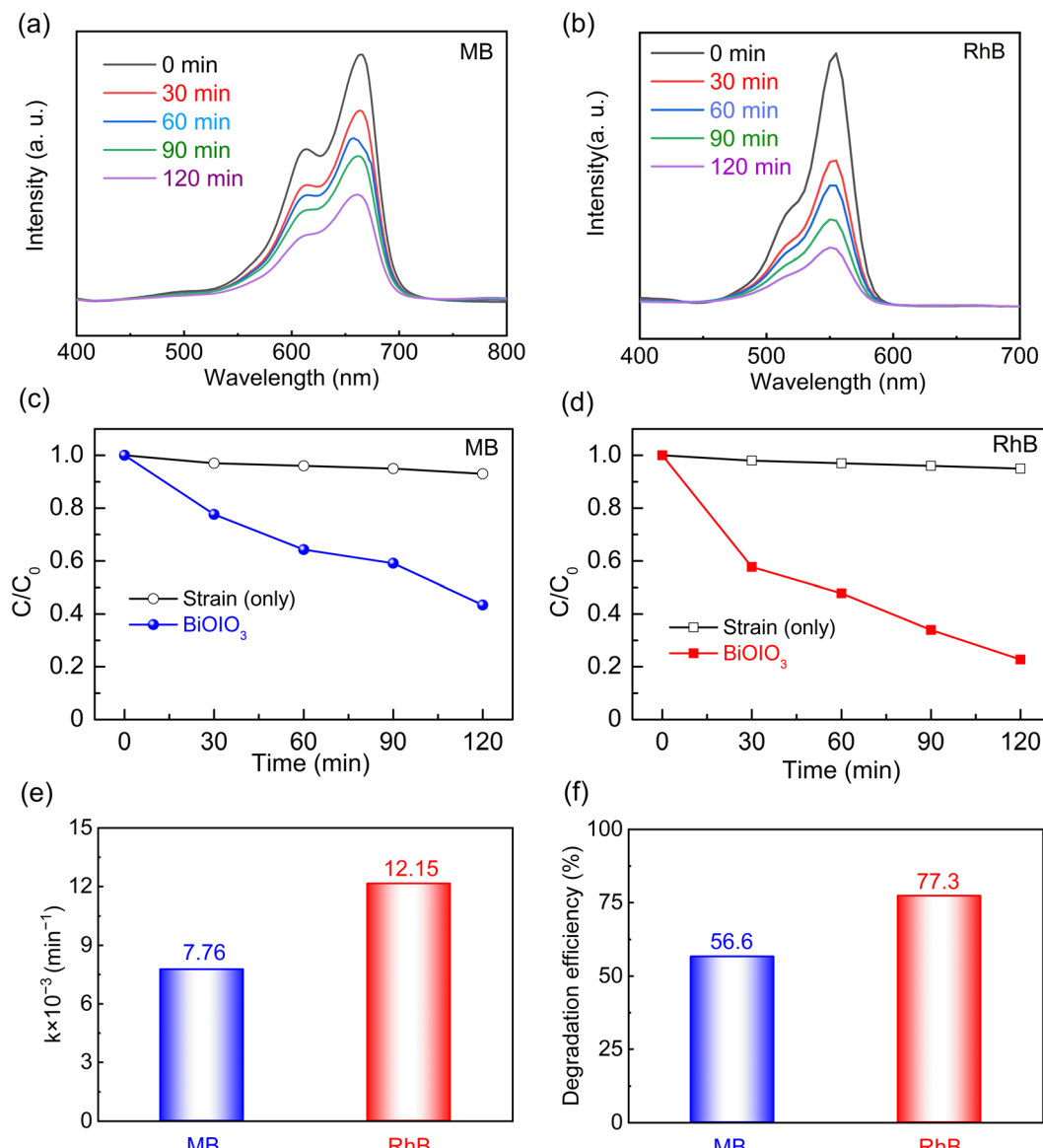


Fig. 2 UV-vis absorption spectra of piezocatalytic degradation for (a) MB and (b) RhB solutions at different time intervals with BiOIO_3 . Piezocatalytic degradation curves (C/C_0 vs. time) of the strain (only) and BiOIO_3 towards (c) MB and (d) RhB solutions. (e) Piezocatalytic degradation kinetic constants and (f) corresponding degradation efficiency of BiOIO_3 towards MB and RhB solutions.

decline may be attributed to the unavoidable loss of catalyst during the cyclic process.³⁵ Additionally, the XRD analysis (Fig. S2) result demonstrates that the structure of the $\text{BiOIO}_3/\text{PMS/US}$ system remains largely unchanged after the cyclic runs, further confirming its excellent stability. Fig. S3 presents the impact of solution pH, ranging from 3 to 11, on the degradation efficiency of RhB in the $\text{BiOIO}_3/\text{PMS/US}$ system, indicating that the degradation efficiency remains relatively stable across all tested pH values. This suggests that the $\text{BiOIO}_3/\text{PMS/US}$ system exhibits a high level of effectiveness for RhB decontamination over a broad pH range.

Tetracycline antibiotics present a significant threat to human health due to their widespread application since their discovery. This extensive use enables these antibiotics to enter aquatic systems through various wastewater sources, including

medical and industrial effluents. Consequently, the removal of tetracycline residues from the environment is essential for safeguarding both ecological integrity and human health.^{36–38} Thus, we investigated the degradation performance of several systems for TC removal, specifically BiOIO_3 , PMS, and the $\text{BiOIO}_3/\text{PMS}$ system, with results presented in Fig. 4(a–d).

Fig. 4(a) presents the TC degradation curves (C/C_0 versus time) for the PMS, BiOIO_3 , and $\text{BiOIO}_3/\text{PMS}$ system under US conditions. The $\text{BiOIO}_3/\text{PMS}$ system also shows a significantly faster degradation activity than that of PMS or BiOIO_3 alone within 10 min. In Fig. 4(b), the $\text{BiOIO}_3/\text{PMS}$ system exhibits the highest k value and the order is as follows: $\text{BiOIO}_3/\text{PMS}$ (0.19837 min^{-1}) $>$ PMS (0.00682 min^{-1}) $>$ BiOIO_3 (0.00476 min^{-1}). Thus, the $\text{BiOIO}_3/\text{PMS}$ system displays superior TC decomposition performance compared to BiOIO_3 alone.



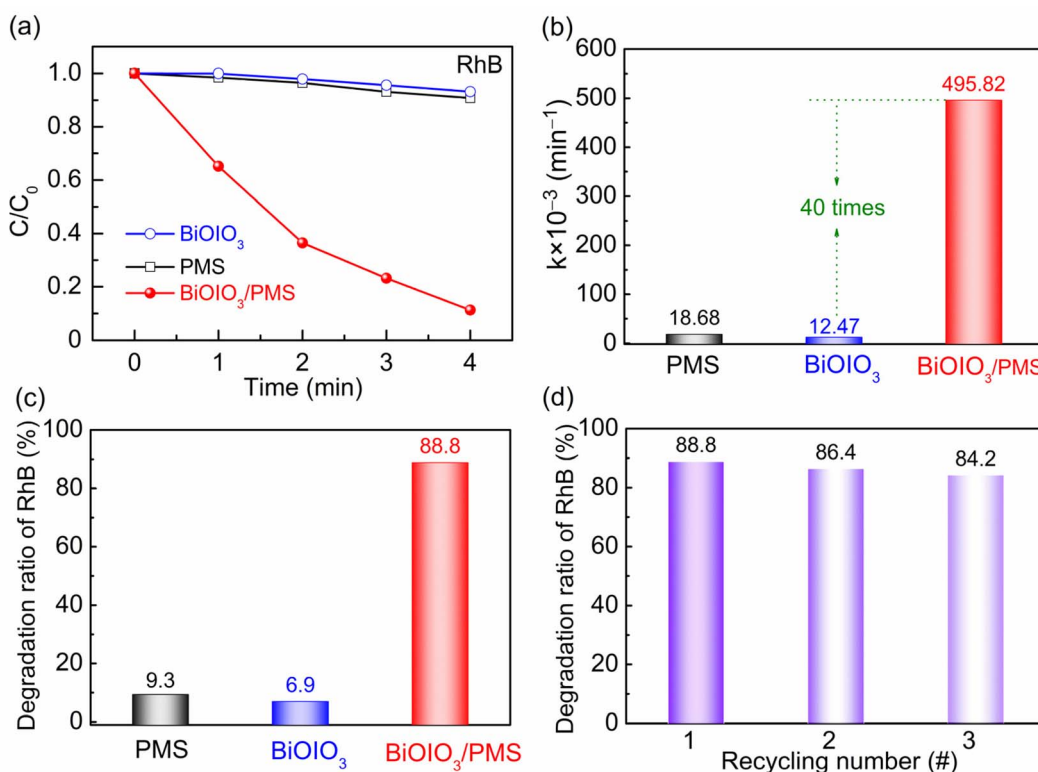


Fig. 3 (a) Catalytic degradation curves (C/C_0 vs. time) of various systems towards RhB solution. (b) Reaction kinetic constants of PMS, BiOIO_3 and $\text{BiOIO}_3/\text{PMS}$ for the degradation of RhB solution. (c) Degradation ratio of RhB (%) for PMS, BiOIO_3 and $\text{BiOIO}_3/\text{PMS}$. (d) Decomposition ratio of $\text{BiOIO}_3/\text{PMS}$ after the recycling tests.

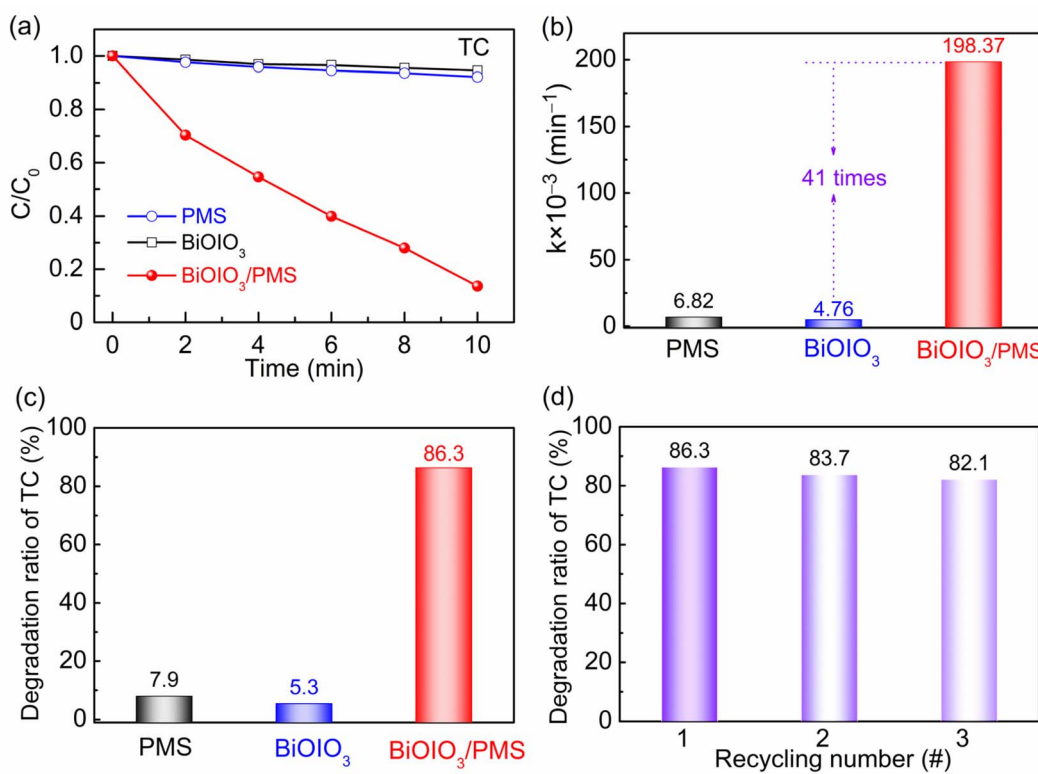


Fig. 4 (a) Catalytic degradation curves (C/C_0 vs. time) of various systems towards TC solution. (b) Reaction kinetic constants of PMS, BiOIO_3 and $\text{BiOIO}_3/\text{PMS}$ for TC solution. (c) Degradation ratio of TC (%) for PMS, BiOIO_3 , and $\text{BiOIO}_3/\text{PMS}$. (d) Degradation ratio of $\text{BiOIO}_3/\text{PMS}$ after the recycling tests.

The results indicate that only 7.9% of TC is degraded after 10 min in the presence of PMS alone, highlighting its limited oxidation capacity. Meanwhile, the use of BiOIO_3 without PMS achieves a mere 5.3% TC removal efficiency. However, the BiOIO_3 /PMS system significantly improves degradation efficiency to 86.3% as shown in Fig. 4(c). Moreover, Fig. 4(d) also proves the good stability of the BiOIO_3 /PMS/US system towards TC in recycling tests. Our findings demonstrate that BiOIO_3 is a highly efficient piezocatalyst for PMS activation in the degradation of organic contaminants, outperforming other recently reported materials systems as displayed in Table S1. Furthermore, this technology toward pollutants degradation over BiOIO_3 /PMS/US system exceeds some single and coupled technologies (e.g. photocatalysis, piezo-photocatalysis, and Fenton-like reactions).^{3,22,28,33}

To further assess the practical applicability of the BiOIO_3 /PMS/US system, we conducted degradation experiments for RhB and TC under real wastewater conditions, as illustrated in Fig. S4(a-b). These results reveal that fluctuations in water quality can somewhat diminish the degradation efficiency of RhB and TC, likely due to the interference of competing inorganic ions with the degradation processes.^{39,40} Overall, the BiOIO_3 /PMS/US system demonstrates excellent removal capabilities for a wide range of contaminants, indicating its potential for effectively addressing pharmaceutical and industrial pollutants in environmental remediation efforts.

Radical scavenging experiments were conducted to study the dominant reactive species generated over the BiOIO_3 /PMS/US system. The experiment aims to elucidate the significance of active species for understanding the piezocatalytic mechanism. Various scavengers were employed to identify the reactive species: 1,4-benzoquinone (BQ) as the $\cdot\text{O}_2^-$ scavenger, *tert*-butanol (TBA) as the $\cdot\text{OH}$ scavenger, methanol (MeOH) as both the $\cdot\text{OH}$ and SO_4^{2-} scavenger and furfuryl alcohol (FFA) as the ${}^1\text{O}_2$ scavenger.^{41,42} Fig. 5(a) indicates that the addition of FFA and MeOH greatly inhibits the degradation of RhB, while BQ and TBA exhibited only minor inhibitory effects. Fig. 5(b) illustrates that the degradation efficiency is markedly affected by the presence of these scavengers, underscoring the vital

influence of reactive species on RhB degradation. The degradation efficiency can be ranked in the following order: control > BQ > TBA > MeOH > FFA. These findings indicate that ${}^1\text{O}_2$, $\cdot\text{OH}$, SO_4^{2-} , and $\cdot\text{O}_2^-$ are involved in the reaction, with ${}^1\text{O}_2$, $\cdot\text{OH}$ and SO_4^{2-} contributing most significantly to RhB removal. In summary, the synergy of non-radical and radical species suggests their adaptability for the degradation of other organic pollutants and highlights their environmental feasibility.

To further confirm the generation of active radicals over the BiOIO_3 /PMS system under ultrasonic vibration, we employed EPR spectroscopy to detect radicals and singlet oxygen. As illustrated in Fig. 6(a), DMPO- $\cdot\text{OH}$ and DMPO- SO_4^{2-} adducts are detected using DMPO as the spin-trapping reagent. These findings suggest that the $\cdot\text{OH}$ and SO_4^{2-} are produced in the piezocatalytic-driven BiOIO_3 system for PMS activation. Besides, the characteristic peaks corresponding to the DMPO- $\cdot\text{O}_2^-$ adduct signal are observed in Fig. 6(b), confirming the generation of $\cdot\text{O}_2^-$. As a potent electrophile, ${}^1\text{O}_2$ can oxidize TEMPO, resulting in the formation of a distinct spin-adduct of TEMPO. In Fig. 6(c), a strong 1:1:1 triplet signal for $\text{TEMPO-}{}^1\text{O}_2$ is detected, with increasing intensity as the reaction progresses, further corroborating the generation of ${}^1\text{O}_2$.⁴¹

Based on experimental results and pertinent literature, a mechanism for the piezocatalytic activation of PMS by BiOIO_3 to enhance pollutant degradation performance is proposed, as shown in Fig. 6(d).⁴³⁻⁵⁰ Initially, the application of external strain by ultrasonic vibration induces deformation and polarization in BiOIO_3 . This deformation generates a piezoelectric field, leading to the separation of electrons and holes. Piezo-generated holes (h^+) can oxidize H_2O , producing $\cdot\text{OH}$. Additionally, h^+ could react with PMS to generate ${}^1\text{O}_2$ and SO_4^{2-} . Concurrently, the piezo-generated electrons (e^-) participate in two vital reactions: one reaction involves the reduction of O_2 to produce $\cdot\text{O}_2^-$, while the other activates PMS to yield SO_4^{2-} and $\cdot\text{OH}$. Furthermore, the generated $\cdot\text{OH}$ and $\cdot\text{O}_2^-$ also contribute to the production of ${}^1\text{O}_2$ within the BiOIO_3 /PMS/US system. Ultimately, the combined action of ${}^1\text{O}_2$, $\cdot\text{OH}$, SO_4^{2-} , and $\cdot\text{O}_2^-$ facilitates the decomposition of pollutants into intermediates that subsequently convert into innocuous products such as CO_2 .

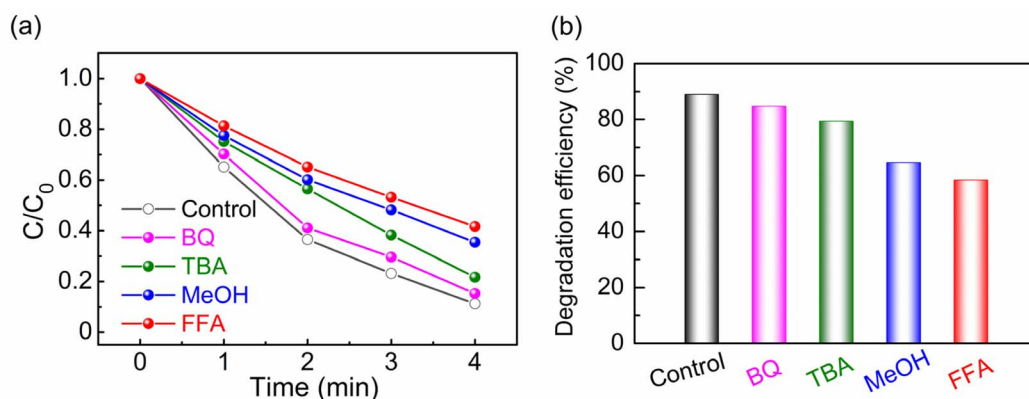


Fig. 5 (a) (C/C_0) -time plots and (b) degradation efficiency of RhB dye over BiOIO_3 /PMS with the various radical scavengers under ultrasonic vibration.



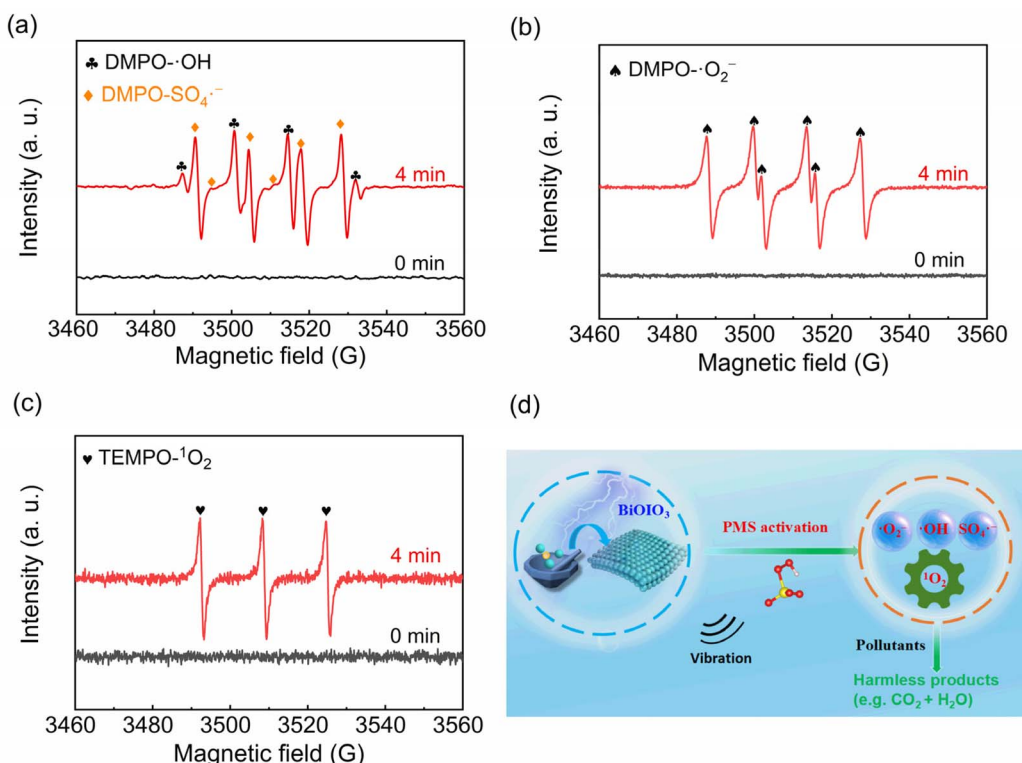


Fig. 6 EPR detection for (a) $\cdot\text{OH}/\text{SO}_4\cdot^-$, (b) $\cdot\text{O}_2^-$ and (c) $^1\text{O}_2$ in $\text{BiOIO}_3/\text{PMS}$ under various ultrasonic vibration conditions. (d) Mechanism of the piezocatalytic activation of PMS for the degradation of pollutants over BiOIO_3 .

and H_2O .⁴⁸⁻⁵⁰ The development of this piezocatalytic AOPs system will not only introduce an innovative technique for PMS reactions but also broaden the application of piezocatalysis in wastewater purification.

4. Conclusions

The BiOIO_3 piezocatalyst was synthesized using a facile solid-state chemical reaction method. A piezocatalytically driven PMS activation system based on BiOIO_3 was established for the degradation of pollutants, demonstrating high degradation efficiency and good stability. These results also prove that the coupled system greatly improves PMS utilization efficiency. Both non-radical and radical species made significant contributions to the piezocatalytic activation of the PMS process. This work presents an effective and straightforward strategy for the removal of wastewater pollutants.

Conflicts of interest

There are no conflicts of interest to declare.

Data availability

The data that support the findings of this study are available from the corresponding author upon reasonable request.

Supplementary information: experimental section (materials characterization and piezocatalytic performances

measurement); XPS survey spectra, other catalytic performances results and comparison of the catalytic performances in this work with recently reported work. See DOI: <https://doi.org/10.1039/d5ra06135k>.

Acknowledgements

The authors gratefully acknowledge financial support from the Talent Introduction Project of Sichuan University of Science and Engineering (No. 2024RC044), National Natural Science Foundation of China (No. 12064042), Scientific Research and Innovation Team Program of Sichuan University of Science and Technology (No. SUSE652A003), Salt City Millions of Talents Program-Leading Team (No. H8012001) and Undergraduate Training Innovation and Entrepreneurship Program of Sichuan University of Science and Engineering (No. CX2025034).

References

- 1 L. Pan, S. Sun, Y. Chen, P. Wang, J. Wang, X. Zhang, J. J. Zou and Z. L. Wang, *Adv. Energy Mater.*, 2020, **10**, 2000214.
- 2 L. Sun, H. Su, Q. Liu, J. Hu, L. Wang and H. Tang, *Rare Met.*, 2022, **41**, 2387.
- 3 X. Qiu, A. Hao, S. Hu, Y. Cao, J. Xie, J. Hu and Z. Lu, *Inorg. Chem.*, 2025, **64**, 6172–6182.
- 4 H. Vuong, D. Nguyen, L. Phuong, P. Minh, B. Ho and H. Nguyen, *Carbon Neutrality*, 2023, **2**, 425–457.
- 5 L. Ju, X. Tang and L. Kou, *Microstructures*, 2022, **2**, 2022008.



6 S. Zhang, H. Zheng and P. Tratnyek, *Nat. Water*, 2023, **1**, 666–681.

7 Y. Zheng, Z. Li, Z. Pan, F. Li, Z. Gao and X. Li, *Chem. Eng. J.*, 2024, **500**, 156570.

8 J. Liu, W. Qi, M. Xu, T. Thomas, S. Liu and M. Yang, *Angew. Chem., Int. Ed.*, 2023, **62**, 202213927.

9 X. Ning, A. Hao, R. Chen, M. F. Khan and D. Jia, *Carbon*, 2024, **218**, 118772.

10 Y. Wang, X. Xu, L. Xiao, L. Li, Q. Xu, Z. Wen, L. Qin, Y. Jia, D. Peng, W. Chen and D. Chen, *J. Adv. Ceram.*, 2024, **13**, 1737–1747.

11 X. Ning, D. Jia, S. Li, M. Khan and A. Hao, *Rare Met.*, 2023, **42**, 3034–3045.

12 X. Li, H. Zheng, J. Liu, H. Li, J. Wang, K. Yan, J. Liu, F. Dang and K. Zhu, *RSC Adv.*, 2023, **13**, 24583–24593.

13 J. Ni, R. Zhao, C. Shi, Y. Ji, A. Hao, A. Xie, H. Yu, S. Boong, H. Lee, C. Zhou and J. Han, *Adv. Powder Mater.*, 2025, **4**, 100265.

14 T. Li, W. Hu, C. Tang, Z. Zhou and Z. Wang, *J. Adv. Ceram.*, 2023, **12**, 2271–2283.

15 J. Yang, M. Zhang, M. Chen and Y. Zhou, *Adv. Mater.*, 2023, **35**, 2209885.

16 S. Liu, B. Jing, C. Nie, Z. Ao, X. Duan, B. Lai, Y. Shao, S. Wang and T. An, *Environ. Sci.: Nano*, 2021, **8**, 784–794.

17 Y. Chen, S. Lan and M. Zhu, *Chin. Chem. Lett.*, 2021, **32**, 2052–2056.

18 S. Tian, Y. Liu, Y. Wang, J. Qi, L. Tian, J. Ma, G. Wen and L. Wang, *J. Hazard. Mater.*, 2022, **433**, 128819.

19 H. Wang, L. Gao, Y. Xie, G. Yu and Y. Wang, *Water Res.*, 2023, **244**, 120480.

20 S. Li, X. Ning, P. Hao, Y. Cao, J. Xie, J. Hu, Z. Lu and A. Hao, *Dyes Pigm.*, 2022, **206**, 110678.

21 F. Cao, L. Yang, Y. Zhang, X. Zhao, H. Lu and J. Wang, *J. Cleaner Prod.*, 2022, **380**, 135002.

22 H. Zheng, Y. Wang, J. Liu, J. Wang, K. Yan and K. Zhu, *Appl. Catal., B*, 2024, **341**, 123335.

23 A. Hao, X. Ning, X. Liu, L. Zhan and X. Qiu, *Chem. Eng. J.*, 2024, **499**, 155823.

24 W. Xu, B. Jing, Q. Li, J. Cao, J. Zhou, J. Li, D. Li and Z. Ao, *J. Mater. Chem. A*, 2024, **12**, 9723–9729.

25 X. Ning, A. Hao and X. Qiu, *Adv. Funct. Mater.*, 2025, **35**, 2413217.

26 X. Ning, A. Hao, Y. Cao, R. Chen, J. Xie, Z. Lu, J. Hu and D. Jia, *Nano Lett.*, 2024, **24**, 3361–3368.

27 J. Xu, H. Che, C. Tang, H. Yang, H. Yang, B. Liu and Y. Ao, *Nano Lett.*, 2025, **25**, 5398–5405.

28 J. Chen, H. Lei, S. Ji, M. Wu, B. Zhou and X. Dong, *J. Colloid Interface Sci.*, 2021, **601**, 704–713.

29 S. Pham, A. Tieu, C. Sun, S. Wan and S. Collins, *Nano Lett.*, 2024, **24**, 3702–3709.

30 Y. Cao, P. Hu, W. Pan, Y. Huang and D. Jia, *Sens. Actuators, B*, 2008, **134**, 462–466.

31 J. Huang, J. Xie, Z. Lu, J. Hu and Y. Cao, *ACS Appl. Nano Mater.*, 2024, **7**, 20206–20216.

32 X. Dong, G. Yao, Q. Liu and Q. Zhao, *Inorg. Chem.*, 2019, **58**, 15344–15353.

33 J. Lai, P. Xiao, Y. Li, S. Cui, J. Yang and H. Lian, *J. Hazard. Mater.*, 2023, **448**, 130908.

34 Y. Zheng, J. Yang, B. Gong, X. Zhang, J. Li, H. Zheng, G. Chen and C. Zhao, *Chem. Eng. J.*, 2022, **441**, 136116.

35 J. Mouljin, A. Diepen and F. Kapteijn, *Appl. Catal., A*, 2001, **212**, 3–16.

36 Y. Liu, S. Liu, M. Chen, Y. Bai, Y. Liu, J. Mei and B. Lai, *J. Hazard. Mater.*, 2024, **461**, 132417.

37 A. Amari, H. Aljibori, M. Ismail, M. Diab, H. Sabban, A. Umarov, S. Madaminov and N. Elboughdiri, *J. Water Process Eng.*, 2025, **70**, 107127.

38 X. Zhang, B. Xu, S. Wang, X. Li, C. Wang, B. Liu, F. Han, Y. Xu, P. Yu and Y. Sun, *Chem. Eng. J.*, 2022, **431**, 133477.

39 M. Rayaroth, G. Boczkaj, O. Aubry, U. Aravind, U. Aravind and C. Aravindakumar, *Water*, 2023, **15**, 1615.

40 X. He, Y. Lu, T. Cai, X. Fu, L. Song, M. Wang, Q. Zeng, Q. Zeng, M. Li, Y. Hua, X. Wu and L. Wang, *J. Hazard. Mater.*, 2023, **457**, 131842.

41 G. Nie, L. Xiao, J. Bi, S. Wang and X. Duan, *Appl. Catal., B*, 2022, **315**, 121584.

42 W. Zhu, C. Wang, X. Li, W. Shi, Q. Chen, X. Bai, F. Fu, D. Wang and C. Yang, *Chem. Eng. J.*, 2024, **499**, 156086.

43 S. Tu, Y. Guo, Y. Zhang, C. Hu, T. Zhang, T. Ma and H. Huang, *Adv. Funct. Mater.*, 2020, **30**, 2005158.

44 P. Jia, J. Li and H. Huang, *Adv. Funct. Mater.*, 2024, **34**, 2407309.

45 J. Roy, D. Mondal, J. Chowdhury, N. Bag, S. Ghosh, S. Roy, R. Mondal, R. Basu and S. Das, *Ceram. Int.*, 2024, **50**, 18012–18023.

46 K. Wang, C. Han, J. Li, J. Qiu, J. Sunarso and S. Liu, *Angew. Chem., Int. Ed.*, 2022, **61**, 202110429.

47 C. Wang, C. Hu, F. Chen, T. Ma, Y. Zhang and H. Huang, *Nano Energy*, 2023, **107**, 108093.

48 T. Jiang, C. Cai, H. Peng, J. Li, X. Fu, C. Nie and Z. Ao, *Chem. Eng. J.*, 2025, **520**, 165824.

49 J. Duan, Y. Li and Z. Zheng, *J. Alloys Compd.*, 2024, **1006**, 176264.

50 H. Wang, Z. Long and R. Chen, *Sep. Purif. Technol.*, 2024, **331**, 125598.

